Saturated ideal modes in advanced tokamak regimes in MAST

IT Chapman[1], M-D Hua[1,2,3], SD Pinches[1], RJ Akers[1], AR Field[1], JP Graves[4], RJ Hastie[1], CA Michael[1] and the MAST Team

[1] EURATOM/UKAEA Fusion Association, Culham Science Centre, Abingdon, Oxfordshire OX14 3DB, United Kingdom
[2] Imperial College, Prince Consort Road, London SW7 2BY, United Kingdom
[3] École Polytechnique, Route de Saclay, 91128, Palaiseau, France
[4] École Polytechnique Fédérale de Lausanne (EPFL), Centre de Recherches en Physique des Plasmas, Association EURATOM-Confédération Suisse, 1015 Lausanne, Switzerland

E-mail: ian.chapman@ukaea.org.uk

Abstract. Plasmas with a safety factor above unity and a profile with either weakly reversed shear, or broad low shear regions, regularly exhibit long-lived saturated ideal magnetohydrodynamic instabilities in MAST. The toroidal rotation is flattened in the presence of such ideal perturbations, and the fast ion losses are enhanced. These ideal modes, distinguished as such by the notable lack of islands or signs of reconnection, are driven unstable as the safety factor approaches the rational value. This could be of significance for advanced scenarios, or hybrid scenarios which aim to keep the safety factor just above rational surfaces associated with deleterious resistive MHD instabilities. The role of rotation, fast ions and ion diamagnetic effects in determining the marginal mode stability is discussed, as well as the role of instabilities with higher toroidal mode numbers as the safety factor evolves to lower values.

1. Introduction

The ultimate goal of magnetic confinement fusion research is to produce steady-state burning plasmas in a fusion power plant. In order to achieve this goal it is necessary to develop a mode of operation in a tokamak which optimises the ratio of the plasma energy to the magnetic field energy (ie maximum β where $\beta = 2\mu_0\langle p\rangle/B_0^2$ and $\langle\cdots\rangle$ represents an averaging over a flux surface and B_0 is the toroidal magnetic field) whilst simultaneously minimising the amount of power required to supply the current non-inductively. So-called 'advanced tokamak scenarios' [1–5] aim to maximise the self-generated non-inductively driven bootstrap current [6] by operating at high plasma pressure and low plasma current. However, the energy confinement degrades with decreasing plasma current, so in order to operate at economically-attractive fusion performance, the energy confinement must be optimised. Furthermore, operating at increased pressure and lower current can lead to deleterious magnetohydrodynamic (MHD) instabilities which would not be unstable with conventional H-mode profiles [7, 8]. Consequently, it is of considerable interest to understand the implications for MHD stability when advanced tokamak profiles are employed.

The two main candidate scenarios for continuous tokamak operation are the steady-state scenario [5], which has reversed magnetic shear in the core, and the 'hybrid' stationary scenario [9, 10], which has a broad low shear region with the safety factor above unity and can operate for long pulse duration in a quiescent state. Here the magnetic shear is a measure of how the magnetic field lines are inclined with respect to one another, $s = r/q\mathrm{d}q/\mathrm{d}r$. The reversed shear (or broad low shear in the case of the hybrid scenario) is a consequence of the optimised bootstrap current which is naturally driven off-axis in regions of strong pressure gradients. Such broad current profiles, together with the peaked pressure profiles required for enhanced plasma performance, result in increased susceptibility to resistive wall modes (RWMs). The RWM is a macroscopic pressure-driven kink mode, whose stability is mainly determined by damping arising from the relative rotation between the fast rotating plasma and the slowly rotating wall mode. In order to achieve a high fusion yield, it will probably be necessary to operate advanced tokamak scenarios with a pressure above the stability limit for RWM onset. Fortunately, recent experiments have shown that this can be achieved in the presence of rotation generated by unidirectional neutral beam injection (NBI) [11–16] or kinetic damping [17–23]. As well as increased susceptibility to RWMs, the advanced tokamak profiles are also often unstable to ideal $n = 1$ kink-ballooning modes, sometimes referred to as infernal modes [5, 7]. Indeed, even if RWMs are not encountered, other MHD instabilities, such as infernal modes or neo-classical tearing modes (NTMs) often inhibit plasma performance at high pressure [24]. Whilst these instabilities do not represent a hard performance limit as they can be avoided by specific tailoring of the plasma profiles, it is important to understand the domains of operation where such MHD instability will occur.

In order to investigate stability in plasmas with advanced tokamak scenario profiles,

MAST typically operates with early NBI heating and low density. By applying early heating, the temperature increases and consequently the plasma resistivity decreases, meaning that the current diffusion time lengthens. As a result of this, the inductively driven current takes sufficiently long to diffuse into the core that the safety factor profile is naturally reversed shear, or broad weak shear, with $q_{min} \sim 1$ for the majority of the discharge. Routine operation at relatively low density is compatible with achieving advanced tokamak q-profiles, whilst a monotonic q-profile with $q < 1$ is obtained when the plasma density is increased. Furthermore, the excellent motional stark effect (MSE) diagnostic measurements of the pitch angle of the field lines gives rise to accurate q-profile prediction with good temporal (< 0.5ms) and spatial (~ 2.5cm) resolution [25,26].

MAST plasmas with an advanced tokamak scenario safety factor profile above unity regularly exhibit long-lived saturated ideal magnetohydrodynamic instabilities. The toroidal rotation is flattened in the presence of such ideal perturbations, and the fast ion losses are considerably enhanced. These ideal modes, distinguished as such by the notable lack of islands or signs of reconnection, are driven unstable as the safety factor approaches the rational value. It is worth noting that the long-term goal of spherical tokamak research is to keep the safety factor well above unity with a significant fraction of non-inductive current drive, hence avoiding such instabilities. Nonetheless, it is pedagogical to study stability with reversed shear safety factor profiles and $q_{min} \sim 1$, in order to provide guidance for stability thresholds in both present and future devices and methods for amelioration of such instabilities.

In section 2, NBI heated plasmas in MAST are described. The phenomenology of the long-living saturated ideal internal mode is outlined, together with differences in observations between different modes of operation of MAST, q-profile evolution and mode number characterisation. The ideal stability of these MAST plasmas is explored in detail in section 3, with particular reference to the role of $\Delta q = q_{min} - 1$, plasma pressure, toroidal mode number and aspect ratio. Section 4 discusses the role of the significant fast ion population in MAST in determining the mode stability, in driving fishbones that precede mode onset and a mechanism of enhanced fast ion losses. The possible physical mechanisms for the damping of the plasma rotation in the presence of MHD activity are explored in section 5, before the implications of this analysis for advanced tokamak scenario operation and the future of spherical tokamaks is discussed in section 6.

2. Experimental phenomenology in MAST

2.1. The long-lived mode

Recent NBI heated MAST discharges often show frequency sweeping n = 1 modes that evolve into a long-lived saturated mode whose frequency evolution is close to that of the central rotation measured by charge exchange recombination spectroscopy. This is illustrated by the Fourier spectrogram of outboard midplane magnetic probe

measurements in figure 1 for MAST discharge 21781. A typical long-lived mode (LLM) has an internal kink structure (not a magnetic island) as can be deduced from the horizontal soft X-ray arrays showing no phase inversion which would be characteristic of a tearing mode. If there is an island present, one would expect that the temperature perturbation would be positive on one side of the island, and negative on the other, resulting in a π-jump in the phase between two radial channels either side of the island. No such phase inversion is observed on the soft X-ray emission, which is correlated to the temperature. However, it should be noted that if the island led to local impurity accumulation, the resultant strong line emission would preclude a phase inversion and so 'hide' the island from diagnostic determination. That said, there is no sign of any local flattening on the high radial resolution Thomson scattering measurements of the electron temperature either, which would occur in the presence of a magnetic island. This in itself is an interesting observation, since saturated modes are often observed to be resistive in their nature. Additionally, the ideal nature of the kink perturbation observed means that it is unlikely that there is a rational surface near the radial location of the kink mode, or else the plasma would be unstable to a resistive-kink at lower plasma β than required for ideal kink instability.

Following the transition from the characteristic fishbone-like behaviour, a reduction in both ion and electron densities and temperatures is generally measured. Furthermore, the energy confinement is degraded following the onset of the LLM. Figure 2 shows that the energy confinement time for MAST shot 17661 is significantly reduced after the appearance of the mode. The confinement time is calculated using the TRANSP [27] Monte-Carlo transport code. In order to match the neutron rate observed experimentally, the anomalous fast ion diffusion rate employed in the transport modelling must be increased by nearly a factor of two, causing the significant degradation in the energy confinement time. The fast ion redistribution in the presence of the LLM is modelled in detail in section 4.3.

The plasma rotation also decreases after the onset of the long-lived mode, as illustrated for discharge 21781 in figure 3. There is a point of inversion, at which the rotation profile remains unchanged. Outside this radius there is a slight increase in the rotation, illustrating a rapid momentum transport ($\sim$10ms) compared to the MAST confinement time ($\sim$50ms). Consequently it is unlikely that either MHD-induced momentum transport or electromagnetic torques associated with resistive effects at resonant layers are responsible for the plasma braking. Moreover, these torques are strongly localised, inconsistent with a simultaneous slowing down of the entire plasma core. The mechanisms responsible for the observed braking are discussed further in section 5.

Following the mode's onset, counter-viewing bolometer measurements show a significant increase, consistent with an enhanced level of fast ion losses, as illustrated in figure 4. A peak in the fast ion losses from the edge channel is seen at each fishbone chirp, and the loss rate increases steadily after LLM onset, even as measured by the core channels. It is rare that the fishbones continue after the LLM has appeared. The

probable reason for this is that the LLM results in a continuous expulsion of fast ions from the core, meaning that the fast ion gradients at the radial location of the inertial layer of the internal kink mode eigenfunction are no longer strong enough to drive fishbones. However, under certain plasma conditions, there are transitions from a saturated long-lived mode state back to fishbones, as reported in reference [28].

2.2. Safety factor profile evolution

The onset of the LLM is inextricably linked to the q-profile evolution. By varying the toroidal field, the evolution of the safety factor has been changed (although other parameters, such as β and ω_* also vary). Since the q_{min} value in the discharges with lower toroidal field evolves to a lower value more rapidly, the LLM onset occurs commensurately earlier. Conversely, MAST plasmas with the highest toroidal field (for the same plasma current) experience the LLM considerably later in the discharge. Figure 5 shows the q-profile for discharge 21781 as reconstructed by the EFIT Grad-Shafranov equilibrium code [29] constrained by the MSE measurement of the field line pitch angle and the magnetic probe measurements on the inboard side of the plasma at a series of time slices during the shot. It is evident that the q-profile exhibits reversed shear throughout the discharge. This is clearly illustrated by figure 6 which shows the magnetic shear $s = r/q\mathrm{d}q/\mathrm{d}r$ as a function of major radius, R, and time. There is always a region of negative magnetic shear, or later a flat profile, in the plasma core. At the time of mode onset (255ms), the safety factor profile is weakly shear reversed and q is above unity everywhere.

This is typical of MAST discharges with early NBI heating and relatively low density. Figure 7 shows the safety factor evolution with respect to major radius and time for discharge 22131 – a good performance MAST plasma with $P_{NBI} = 3.5$MW and $\beta_N = 2.7$, toroidal field $B_T = 0.4$T and plasma current $I_P = 820$kA. Again, it is clear the the q-profile is always above unity and exhibits reversed shear for the duration of the discharge. Naturally, the safety factor in these MAST discharges in the absence of any off-axis non-inductive current drive schemes is only transient and would eventually evolve to become monotonic as the current diffuses into the core. Nonetheless, such conditions provide an excellent testing ground for the stability of advanced tokamak scenarios since the q-profile is naturally reversed shear tending towards a hybrid like scenario with broad low shear towards the end of the pulse.

In some cases, for instance discharge 21781 shown in figure 5, the q-profile determined by the EFIT reconstruction constrained by the MSE measurements suggests that $q_{min} < 1$. Indeed, even if the EFIT prediction is constrained by the Thomson scattering measurements for the electron density and temperature and the charge exchange measurement of the ion temperature, q_{min} is predicted to be just below unity. However, the uncertainty in these measurements leads to an error bar on the safety factor. If the q-profile had evolved to below unity, at such large β_p and r_1, the plasma would be highly unstable to the resistive kink mode. Even in the presence of fast ions and

strong toroidal rotation, it would be expected that the plasma would exhibit sawtooth oscillations if $q < 1$. In these plasmas where the LLM saturates and no reconnection occurs, it is probable that q_{min} remains above unity. Indeed, it could be postulated that the plasma eventually disrupts, as is often observed, when the current eventually diffuses into the core and the $q = 1$ surface enters the plasma, allowing the resistive kink mode to trigger a giant sawtooth crash. Since the radial position of the $q = 1$ surface when it appears is so broad in MAST plasmas with a wide low-shear region, the stored energy within $q = 1$ means that upon a sawtooth crash the perturbation is sufficiently large to disrupt the plasma.

2.3. Toroidal mode number analysis

Figure 8 shows the toroidal mode numbers calculated from the Fourier spectrogram of outboard midplane magnetic probe measurements for MAST shot 21781. It is clear that during the saturated phase of the LLM evolution there are $n = 1$, $n = 2$ and $n = 3$ harmonics present. It is possible to estimate the relative amplitudes of different toroidal mode number instabilities during the LLM evolution from the soft X-ray fluctuation data. By taking a fast Fourier transformation of the soft X-ray data for each vertical line of sight, the amplitude of the fluctuation can be calculated as a function of frequency. The spectrum has a peak at the $n = 1$ mode's frequency and a secondary peak at twice this frequency from the $n = 2$ mode. At the time of the mode onset, the amplitude of the peak at the $n = 1$ frequency is two orders of magnitude larger than the peak at twice the frequency. It is possible to determine the relative amplitude of the $n = 2$ mode with respect to the $n = 1$ mode by comparing the amplitudes of the peaks in the spectrum. This is only possible since the linear MHD stability analysis indicates that both the $n = 1$ and $n = 2$ displacements are peaked at the same radial location, that of the q_{min} surface.

Figure 9 shows the temporal evolution of the relative amplitude of the $n = 2$ mode compared to the $n = 1$ mode for MAST discharge 21781. It is clear, that at first the LLM has a purely $n = 1$ character. However, as the safety factor evolves and Δq decreases, the $n = 2$ mode increases in amplitude rapidly and becomes of comparable amplitude as the $n = 1$ mode. It should be noted that the fast Fourier transformation does results in coupling to higher toroidal mode numbers due to the toroidicity of the tokamak plasma. However, the fact that the ratio of the $n = 2$ amplitude compared to the $n = 1$ mode changes does suggest that the higher-n harmonics observed in figure 8 are due to changes in mode stability rather than artifacts of the Fourier transformation.

2.4. Phenomenology of the LLM in various MAST plasmas

The long-lived mode is often observed in MAST plasmas heated by neutral beam injection during the current ramp and consequently exhibiting reversed shear q-profiles with $q_{min} \sim 1$. Whilst the fundamental characteristics of the mode (viz. flattening of the rotation profile, enhanced fast ion losses, decreased neutron rate) are always present,

the mode behaviour does vary. Notably, the onset time, the duration of the saturated phase, which can approach half of the plasma duration, the rate of braking and the severity of the deleterious mode effects are dependent upon other plasma parameters such as Δq and β_p and on the plasma scenario exploited. For instance, it is observed that the LLM onset is dependent upon the plasma density. If the density is raised sufficiently high, MAST plasmas do not experience the long-lived mode, but are instead subject to sawtooth oscillations, indicating that the $q = 1$ surface has definitely entered the plasma. Similar MAST discharges (matched plasma current $I_p = 750$kA, toroidal field $B_T = 0.58$T, and beam heating $P_{NBI} = 1.8$MW from 70ms) have been performed for a range of plasma densities. Raising the density has two key effects on the stability of the $n = 1$ internal mode. Firstly, the higher density results in a reduced plasma temperature which means that the plasma resistivity increases, so the current diffusion time decreases. The result is that the current diffuses into the plasma core more rapidly and the safety factor evolves to a state below unity more rapidly. When this happens, the presence of the q=1 rational surface allows reconnection and the plasma is resistively unstable. Such a state inevitably results in sawtooth oscillations. Secondly, a higher order effect of increased density is to change the beam ion deposition significantly. The slowing-down time of the NBI fast ions is decreased with increasing density. The enhanced collision rate results in a fast particle population which has more ions at lower energy and more ions at larger radius. This reduces the spatial gradient of the distribution function, f_h, at the radial location of the mode (drive) and increases the velocity gradient of f_h (damping).

The onset of the mode can also be significantly affected by altering the beam heating waveform around the time of LLM appearance. Figure 10 shows three different shots with the same plasma current, toroidal magnetic field and density and a window in the neutral beam heating around 250ms – the time of mode onset in a similar plasma with continuous heating. In shot 21792 the beam heating ceases during the LLM phase. At this point the amplitude of the mode drops due to the reduction in β and it subsequently disappears. Since the temperature drops and therefore the resistivity increases, the safety factor is now able to continue to evolve below one. The appearance of the $q = 1$ surface is confirmed by the first sawtooth crashes at 263ms and 275ms which exhibit not only a drop in the core soft X- ray emission but a clear increase in the edge channel, symptomatic of a reconnection. After the beam heating recommences, the sawteeth predictably lengthen in period due to the presence of fast ions and enhanced rotation [30, 31], but the LLM does not return. In contrast, in shot 22080 the LLM has not appeared when the first beam is switched off. It only appears at 265ms after the beams are switched on again and, accordingly, the plasma β has sufficiently increased. Finally in shot 22082, the beam is switched off again just before the LLM onset. This time however q_{min} has dropped far enough, and the β is still sufficiently large, that the LLM is driven unstable at 240ms, even though the beam heating has ended. The mode soon drops in amplitude as the plasma pressure falls in the Ohmic phase, and grows in amplitude again once the heating recommences.

MAST has recently operated in a significantly vertically displaced lower single null configuration in order to test off-axis neutral beam current drive predictions [32]. These single null plasmas do not suffer from long-lived modes, but usually exhibit sawteeth. There are two primary factors which influence this behaviour. Firstly, the fast ion distribution function is peaked well off-axis. It has been shown that if the fast ion population is peaked near the internal mode's radial location, the passing fast ions can significantly influence the stability of the internal kink mode [33–35]. Secondly, the off-axis neutral beams drive a significant non-inductive current. Whilst this neutral beam driven current is not sufficiently localised to result in a significant change in the magnetic shear at the $q = 1$ surface which would affect the sawtooth behaviour, it does lead to a change in the q-profile. By driving current off-axis near the radial location of q_{min}, the safety factor drops below unity much earlier in the single null plasmas. It is important to remark that in these off-axis plasmas it could also be anticipated that the fast ions would destabilise the kink mode should it be unstable with positive Δq. Indeed, the passing fast ions born outside the q=1 surface do strongly destabilise the internal kink mode, manifest as a shortening of the sawtooth period [36]. Since the LLM has the same eigenstructure as the mode responsible for sawteeth (except for the tearing at the rational surface which does not strongly influence any fast ion stabilisation mechanisms), it could be anticipated that fast ions will also play a key role in determining the LLM stability (though notably only the threshold criterion, not the saturation level).

Finally, the LLM is also usually absent in plasmas when the neutral beam is directed in the opposite direction to the plasma current. Once more, there are multiple contributory factors to this observation: Intrinsic error fields necessitate that MAST counter-NBI plasmas are usually operated at very high plasma density to avoid triggering locked modes, and consequently operate at low temperature. At such low temperatures, the resistivity is higher allowing the current to diffuse into the plasma core and the safety factor to evolve to a state below unity more rapidly. This is manifest by sawtooth oscillations which are usually observed in counter-NBI discharges. The internal mode can also be driven more unstable by the presence of energetic counter-propagating ions [31,37]. Furthermore, when the fast ions are injected counter to the plasma current they experience a ∇B drift in the opposite direction to co-propagating ions. This means that their orbits experience an outward drift which has two significant effects on kink mode stability. The first is that the fast ion confinement is poor and there are large first orbit losses, reducing the effect of fast ions. These enhanced first orbit losses also result in a return current, and so the increased torque leads to faster rotating plasmas with broader rotation profiles. The second ∇B drift effect is that the distribution function is peaked more off-axis, which can be significant in kink mode stability.

3. Stability in weak and reversed shear MAST plasmas

The fact that no island is observed in the soft X-ray emission or the Thomson scattering profiles suggests that the saturated n=1 internal mode is an ideal MHD mode. This

ideal instability occurs despite the absence of a q=1 surface from the plasma at the time of mode onset. If there were a q=1 surface, the negative helical flux of the safety factor profile would permit tearing and reconnection. In such circumstances the resistive kink mode becomes unstable at lower plasma pressure than the ideal mode, and is usually manifest in MAST plasmas as sawtooth oscillations.

The MAST plasma reported here all exhibit reversed shear q-profiles early in the discharge, evolving to 'hybrid' like profiles with a broad low-shear region, as illustrated in figures 5, 6 and 7. In the region of negative shear the plasma becomes unstable to the $n = 1$ internal kink mode, even at zero poloidal beta, $\beta_p = p/(B_a^2/2\mu_0)$, where $B_a = \mu_0 I/l$ and l is the poloidal perimeter of the plasma. In equilibria with reversed shear, strong pressure gradients near the radial position of q_{min} can destabilise low (m, n) ideal modes with m/n near q_{min}, where m and n are the poloidal and toroidal mode numbers respectively. In plasmas with broad low-shear regions, the pressure profile is typically less peaked, and so these instabilities are avoided. However, as the q-profile evolves to become broad and flat and the β increases too much, the plasma becomes unstable to the so-called infernal mode – a low m/n kink-ballooning mode with $m/n \approx q$. Indeed, it is quite conceivable that the LLM sometimes results with an infernal mode structure if Δq evolves down towards one much quicker than β_p increases such that the internal kink mode is never unstable, or if the rotation and fast ion effects keep the internal kink stable. Whilst the internal kink and infernal modes have different driving mechanisms, they would both produce a displacement of the plasma, and the saturation for either eigenstructure could result from the field-line bending term dominating at a finite displacement amplitude provided the rational surface at the mode's location does not enter the plasma and allow reconnection.

3.1. Internal kink mode stability

Theoretical analysis [38] for a large aspect-ratio cylindrical approximation shows that reversed shear q-profiles typical of MAST plasmas are unstable to the $n/m = 1/1$ internal kink mode, even with zero plasma β. The growth rate of the $n = 1$ internal kink mode for a non-monotonic q-profile with $q > 1$, $q(r_1) = q_{min}$, $q'(r_1) = 0$, $\Delta q = q(r_1) - 1$ has been derived [38] as

$$\bar{\gamma}\Big[1 + \frac{\Delta q}{\bar{\gamma}}\Big]^{1/3} = \frac{1}{(r_1^2 q'')^{1/3}}\Big[- \pi \frac{r_1^2}{R^2}\delta W^{MHD}\Big]^{2/3} \tag{1}$$

where $\bar{\gamma} = \sqrt{3\gamma^2/\omega_A^2 + (\Delta q)^2}$, the Alfvén frequency is $\omega_A = v_A/R$, $v_A = B_0/\sqrt{\mu_0 \rho_0(r_1)}$ and the fluid mode drive, δW^{MHD}, is given in references [38] and [39]. Thus, when the q-profile evolves such that q_{min} approaches unity (but remains greater than one), the $n = 1$ internal kink has a finite growth rate. As the q-profile evolves, this mode will saturate nonlinearly, provided that q remains greater than one. Since the absence of negative helical flux prohibits reconnection, the stabilising field-line bending term begins to dominate over the fluid drive as the perturbation amplitude increases. When this point is reached, the perturbation saturates. Nonlinear analytic calculations [40, 41],

again in the circular, large aspect ratio limit, have shown that the saturated amplitude can be related to the linear growth rate, as

$$\xi^2 q'' = \frac{8}{71}\Big(\frac{8\pi}{3}\Big)^2\Big[\Big(\frac{\Delta q_{crit}}{\Delta q}\Big)^{3/2} - 1\Big] = \frac{15}{71}\Big(\frac{8\pi}{3}\Big)^2\Big[\frac{\gamma^2}{\omega_A^2}\Big] \tag{2}$$

where ξ is the radial displacement of the core plasma and the critical Δq for which the $n = 1$ internal kink mode is unstable is given by

$$\Delta q_{crit} = (2r_1^2 q'')^{-1/3}\Big(\frac{\pi r_1^2 |\delta W^{MHD}|}{R^2}\Big)^{2/3} \tag{3}$$

3.2. Infernal mode stability

The q-profile in the 'hybrid' scenario [9, 10] exhibits a wide region of practically zero magnetic shear, as do q-profiles in other advanced scenarios with elevated magnetic shear [42]. Under these circumstances, and coupled with the high plasma pressures desirable in such advanced scenarios for optimal fusion performance, the plasma is unstable to internal, ideal kink-ballooning modes. The stability of low shear plasmas for $m = n$ has been investigated analytically in references [43, 44] and for arbitrary m, n in reference [45]. For a low-shear q-profile with a radius $r = r_1$ separating the low-shear inner region where $q = q_r + \Delta q$, $q_r = m/n$ and $\Delta q \sim \epsilon$ from the other region where q is assumed to increase to $q = q_a \gg q_r$, the growth rate of the infernal mode is found [43,45] to be

$$\Big(\frac{\gamma}{\omega_A}\Big)^2 = \frac{n^2}{1 + 2q_r^2}\Big[\frac{2\epsilon_1^2\beta_p^2\Lambda_{m,n}}{(m+1)^2(m+2)} - \Big(\frac{\Delta q}{q_r}\Big)^2\Big] \tag{4}$$

where this equation holds for both positive and negative Δq [46] and $\Lambda_{m,n}$ represents the coupling between m and $m \pm 1$ sidebands,

$$\Lambda_{m,n} = \frac{m+1}{2}\frac{m + 2 + C_{m+1,n}}{m - C_{m+1,n}} \tag{5}$$

and $C_{m+1,n} = r\xi'_{m+1,n}/\xi_{m+1,n}$. This analytic stability analysis is valid only in the large aspect-ratio limit and for parabolic pressure profiles, $p(r) = p_0(1 - r^2/r_0^2)$. Including the effects arising from toroidal rotation, and taking $q_r = 1$, the growth rate equation becomes

$$\frac{\gamma^2}{\omega_A^2} = \frac{n^2}{3}\Big[\frac{2\epsilon_1^2\beta_p^2\Lambda}{(m+1)^2(m+2)} - \Delta q^2\Big] - \frac{\omega_{BV}^2}{\omega_A^2} \tag{6}$$

where the Doppler Shifted mode frequency $\omega_D = \omega_{r+i}\gamma + \Omega(r_1)$ and

$$\omega_{BV} \approx \frac{\mathcal{M}^2\Omega^2}{1 + 2q_s^2}\Big[(1 - \frac{1}{\Gamma}\Big] \tag{7}$$

with the Mach number $\mathcal{M} = \rho\Omega^2 R_0^2/2p$. Note that $\omega_{BV} = 2\mathcal{M}^2\Omega^2/15$ for $\Gamma = 5/3$ and $q_r = 1$.

In order to express equation 6 in terms of parameters which can easily be quantified and varied experimentally, the β_p terms can be written in terms of normalised beta, $\beta_N = \frac{\langle\beta\rangle}{I_N}$ where $I_N = \frac{I\mu_0}{aB_0}$ and $\langle\beta\rangle$ is the volume average beta. Note that $I_N \approx \epsilon_a/q_a$ so

that $\beta_N \approx \langle\beta\rangle q_a/\epsilon_a$. For the pressure profile employed here, $\beta_p = \beta_0/2 \cdot R_0^2/r_0^2$. Finally let us define the peaking factor P_k as $P_k = P_0/\langle P\rangle$ and so

$$\beta_p = \frac{q_s^2}{q_a}\beta_N \frac{P_k^2}{4\epsilon_a} \tag{8}$$

Solving analytically the homogeneous cylindrical quasi-linear second order differential equation for C_m [47] we obtain for $q_s = 1$ and $q_a >> 1$,

$$\Lambda_{m,n} = \frac{(m+1)(m+2)}{2m(2m+1)} q_a \Big(\frac{r_1}{a-r_1}\Big)^2 \tag{9}$$

The result of this stability analysis is that the infernal mode is unstable in plasmas with broad low-shear q-profiles for $m = n$ and $w_r = \Omega(r_1)$ when

$$\frac{\gamma^2}{\omega_A^2} = \frac{m^2}{3}\Big[\Big(\frac{\hat{\rho}^2}{1-\hat{\rho}}\Big)^2 \frac{\epsilon_a \beta_N P_k^2}{4m(m+1)(m+2)} - \Delta q^2\Big] - \frac{\omega_{BV}^2}{\omega_A^2} \tag{10}$$

where $\hat{\rho} = r_1/a$. This means that increasing the beta raises susceptibility to infernal modes, as does widening the region of low magnetic shear, since $\Lambda_{m,n} \sim r_1^2/a^2$. Of course, in spherical tokamaks like MAST, β_p is naturally higher and the region of low-shear is typically very large, extending well beyond mid-radius, making ST plasmas with $q_{min} \sim 1$ susceptible to ideal infernal modes. The highest growth rates are achieved for $m = n$ modes, typically an order of magnitude greater linear growth than $m > n$ modes. It is also of note that the 2/2 mode can have a higher growth rate than the 1/1 mode for $q_{min} \approx 1$, although it is only unstable across a smaller range of Δq. The critical Δq for which the $m = n$ infernal mode is unstable can be found from equation 6 as

$$\Delta q_{crit} = \Big[\frac{3}{m^2}\Big(\frac{\omega_{BV}^2}{\omega_A^2} - \frac{m^2}{3}\frac{2\epsilon_{1^2}\beta_p^2\Lambda_{m,n}}{(m+1)^2(m+2)}\Big)\Big]^{1/2} \tag{11}$$

3.3. Stability with respect to Δq

The linear stability of the n=1 internal mode has been assessed for the evolving q-profile exhibited in MAST plasmas. The q-profile has been reconstructed for discharge 21508 by constraining the EFIT [29] equilibrium reconstruction with the MSE field line pitch angle measurements and the magnetic probe measurements on the inboard side. The equilibrium is then produced by the HELENA code [48] and the linear stability of this equilibrium is found using the CASTOR MHD code [49]. In order to find Δq_{crit} (as defined by equation 3 for a circular large aspect-ratio plasma), the safety factor on-axis has been scaled by varying the toroidal magnetic field, and the linear growth rate of the internal mode has been found for a range of Δq. The equilibrium is reconstructed at the time of the LLM onset and the q-profile is scaled arbitrarily to retain the same q-profile shape whilst varying Δq in order to assess the role of the minimum in the safety factor in determining the mode stability, independent from the exact details of the current density distribution. Figure 11 shows the $n = 1$ mode growth rate for a range of q_{min}. It is evident that the mode is stabilised as the safety factor is raised above unity. However, the internal mode has a finite growth rate for Δq up to 0.12, which

represents a significant period of time during the q-profile evolution in MAST. This means that there is substantial scope for an ideal internal mode to be driven unstable, even with $q > 1$.

By reconstructing the equilibria for discharge 21781 at a number of time slices during the pulse, the linear stability of the $n = 1$ mode is assessed temporally using the MISHKA-1 reduced-MHD stability code [50]. Each HELENA equilibrium reconstruction is constrained by the MSE measurements and uses the last-closed flux surface shape, β_N and q_0 from EFIT. Figure 12 shows the growth rate of the $n = 1$ mode as a function of time. It is evident that the ideal $n = 1$ internal mode becomes unstable at approximately the same time as the LLM appears experimentally (see figure 1). The mode is driven unstable primarily by the decrease in Δq rather than an increase in plasma pressure. Indeed, if the stability of an equilibrium with the q-profile at the time of mode onset is assessed with negligibly small β, the $n = 1$ internal mode is still unstable, exemplifying that, at least for discharge 21781, the Δq parameter governs the instability drive. The exact point of marginality does not agree, most probably due to second order stabilisation effects from the toroidal rotation, the presence of fast ions or ion diamagnetic effects. Nonetheless, the excellent accordance between the experimental observation of mode onset and the time at which the ideal $n = 1$ mode is found to be unstable suggests that, to leading order, the mode stability can be assessed using ideal MHD theory.

The long-lived mode is only ever observed in MAST plasmas heated by neutral beam injection. The beam heating has three primary influences on the MHD stability of the plasma: firstly it raises the temperature, which reduces the resistivity and allows the q-profile to evolve to the reversed shear or weakly sheared regime with $q_{min} \geq 1$ as illustrated in figures 5, 6 and 7; secondly, the NBI increases the plasma β which makes the mode more linearly unstable; and thirdly, the increased pressure enhances the bootstrap fraction, helping to sustain the advanced tokamak safety factor for a longer time. It is possible to assess the role of the plasma pressure in determining the point of marginal stability for these ideal low-n internal modes. Figure 13 shows the growth rate of the $n = 1, 2, 3$ internal modes as a function of β_p for a fixed $\Delta q = 0.02$. It is clear that with these reversed shear profiles, the ideal $n = 1$ internal mode is driven unstable, even at zero beta, as expected theoretically [38]. However, the LLM does not appear, even in plasmas with a sustained reversed shear q-profile above unity if the performance is poor. For instance, figure 10 shows discharge 22080, where the $\Delta q \leq 0.1$ during the window without NBI heating, when the LLM is absent. The mode onset only occurs once the NBI recommences and the β_p increases. This illustrates that whilst ideal MHD can accurately predict the onset of the mode at high β, as shown by comparing figure 1 with figure 12, non-ideal stabilisation effects can be significant in determining the point of marginal stability at modest plasma pressures. When the β is small, the linear growth rate of the $n = 1$ mode is predicted to be small, so the strong toroidal rotation present in MAST plasmas could be anticipated to stabilise the mode.

3.4. Rotation effects

The rotation in spherical tokamaks such as MAST can approach the ion sound speed and is typically of the order of $v_0/v_A \sim 0.4$ due to the small moment of inertia of the plasma and large beam power per unit volume. It has been shown analytically [51, 52] and numerically [30] that strong toroidal rotation can stabilise the internal kink mode. It is possible to use the MISHKA-F code [53] to assess the stabilisation of the $n = 1$ internal mode due to the presence of such strong toroidal rotation. MISHKA-F employs the static equilibrium generated by the HELENA code and includes the toroidal rotation perturbatively in the stability analysis. Whilst it has been shown [54] that such inconsistent inclusion of the equilibrium rotation can lead to errors in the calculation of the mode growth rate, the critical flow required to marginally stabilise the mode is always overestimated, so this represents an appropriate test of the importance of the role of flow. Figure 14 shows the growth rate of the $n = 1$ internal mode with respect to the toroidal rotation at q_{min} for different poloidal beta values. At the time of mode onset in the experimental plasma the poloidal beta is $\beta_p = 0.43$. Since we are interested in the role of rotation in determining the marginal stability of the mode, the rotation profile used is that measured experimentally by charge exchange spectroscopy at the time of the LLM onset. It is clear that whilst the toroidal rotation is expected to have a stabilising influence upon the $n = 1$ internal mode, the experimental level of flow can only completely suppress the mode at low plasma pressure. This may explain why the LLM is not observed in low pressure plasmas with reversed shear q-profiles despite the internal mode being ideally unstable at zero β. It is worth noting that recent work has shown that this stabilisation is strongly dependent upon the equilibrium density and rotation profiles [55]. Thus, once the fluid drive of the internal kink becomes sufficiently strong to overcome the rotational stabilisation, the effect of flow is quickly diminished as the mode itself flattens the rotation and enhances its growth. This interaction between the toroidal rotation and the presence of MHD instabilities is discussed in reference [56] and will be the focus of future nonlinear stability analysis. In future spherical tokamaks, such as the Components Test Facility (ST-CTF) [57–59] where the toroidal rotation may be significantly larger, the stability to the LLM in these advanced tokamak regimes may be improved.

3.5. Evolution of the saturated internal mode

It was shown in section 2.3 that the LLM begins with a purely $n = 1$ character, but evolves to have increasing $n = 2$ and $n = 3$ components which become comparable in amplitude to the $n = 1$ harmonic. Figure 15 shows the growth rate of the internal mode with respect to Δq for $n = 1, 2, 3$. It is clear that the $n = 1$ mode is unstable for a wider range of Δq than $n = 2, 3$ modes. However, the higher-n modes become progressively more unstable at a sufficiently small Δq. It is possible to infer from figure 12 that as q_{min} drops, the plasma first becomes unstable to the $n = 1$ kink mode, as observed experimentally. As the current continues to diffuse and the safety factor drops,

the $n = 2$ mode in driven unstable, and finally the $n = 3$ mode becomes unstable. This appears to be in excellent agreement with the empirical observations (as illustrated in figure 9), at least qualitatively. Furthermore, analytic calculations [45] suggest that for very broad low-shear regions present in these MAST discharges as $q_{min} \rightarrow 1$, the higher-n infernal modes become more unstable that the $n = 1$ harmonic. Such excellent agreement between the experimental signatures and the analytic and numerical analysis suggests that the interpretation of the LLM as an ideal saturated infernal mode late in its evolution is robust. The eigenfunctions for the $n = 1, 2, 3$ internal modes for MAST shot 21781 when $\Delta q = 0.02$ are shown in figure 16, indicating the low-n kink-ballooning structure typical of infernal modes in low-shear, high-β plasmas. Whilst it is not possible to compare the linear growth rates with the nonlinear saturated amplitude of the modes, such a linear analysis does offer a qualitative insight into the plasma behaviour. Nonlinear MHD stability modelling will be the subject of future research.

Finally, it is possible to estimate the saturated mode amplitude using data from the Soft X-ray cameras. The structure of the long-lived mode is first determined using the CASTOR linear code [49] with zero resistivity, a setting justified by the absence of any island in the plasma, and its saturated amplitude is estimated by comparing results of the forward analysis of the soft X-ray emission to experimental data. The calculation is done for many arbitrary toroidal numbers, and in complete toroidal geometry, thus including a full spectrum of poloidal numbers. It is based on the equilibrium constrained to the pressure from Thomson scattering and charge exchange measurements, and the field line pitch angle from the MSE. The simulated soft X-ray emissivity is given by the theoretical expression of bremsstrahlung emission, $\epsilon_{SXR} \propto (n_e n_i Z_{eff}^2/\sqrt{T_e}) \int \exp(-h\nu/T_e) \mathrm{d}\nu$ where n_i, n_e, and T_e are the ion density, electron density and temperature measured by the charge exchange and Thomson scattering respectively, and assuming electroneutrality, ν is the emission frequency and Z_{eff} is obtained by analysis of the bremsstrahlung emission on an equilibrium timescale. The shape of the flux surfaces can be inferred from the equilibrium field, the magnetic perturbation and its assumed amplitude. Since the resulting structure rotates toroidally, it produces fluctuations measured by the soft X-ray cameras. For the simulation, this rotation is deduced from the measured soft X-ray data by cross-correlation techniques. This allows the mapping of the distorted flux surfaces seen by the cameras, hence the simulation of the line integrated soft X-ray measurements. This forward analysis is carried out for different mode amplitudes and compared to the experimental data. Since the MHD perturbation does not affect the average soft X-ray signal but only results in its variation, the comparison with the experimental data is based on this fluctuation only. This method reduces the influence of parasitic soft X-ray sources, such as impurity line emission. Further details can be found in reference [56]. Fluctuations observed on the soft X-ray cameras are consistent with a saturated radial amplitude of 1.2cm. In comparison, equation 2, although only valid for large aspect ratio, circular plasmas, predicts a saturated amplitude of 4.5mm.

3.6. Aspect ratio and shaping effects

The saturated internal ideal mode, and consequently the resultant deleterious effects associated with the mode, is more prevalent in spherical tokamaks than in conventional aspect-ratio devices for two reasons: Firstly, since the stability of the internal kink mode is determined by a term in δW which is of the order $O(\epsilon^2)$, this term is much larger for tight aspect ratio. The result of this is that the internal kink is driven unstable at a much larger value of q_{min} (see equation 3 for Δq_{crit} containing $\delta W^{2/3}$ in the numerator). Secondly, since the q-profile is typically rather broad in spherical tokamaks, it means that when q=1 does finally enter the plasma, r_1 will be very wide, usually extending beyond mid-radius, which results in a substantial drive for the $n = 1$ kink mode, leading to large, often disruptive, sawteeth. In order to assess whether such internal modes will beset conventional aspect ratio devices in advanced tokamak regimes, the effect of the equilibrium inverse aspect ratio on the $n = 1$ growth rate has been modelled. Figure 17 shows the growth rate of the $n = 1$ internal mode with respect to the inverse aspect ratio, $\epsilon = a/R$. The equilibria are generated with HELENA and the MHD stability is found using MISHKA-1. The poloidal beta is fixed throughout the scan, which means that the resultant Δq does vary. It is clear that the mode is more unstable in the tighter aspect ratio configuration, but that there is a finite growth rate for the conventional aspect ratio case ($\epsilon \sim 0.3$). However, since the proximity of the minimum in the safety factor to the rational surface has been shown to be the dominant factor in determining the mode stability, it is also of interest to assess the range of Δq over which the ideal internal mode is unstable. Figure 18 shows the growth rate of the $n = 1$ internal mode as a function of Δq for different inverse aspect ratios. The plasma is unstable to this mode for a larger range of Δq in the low aspect ratio case. Nonetheless, the conventional aspect ratio plasma is also unstable to such internal modes when $q_{min} \rightarrow 1$, as is the case in 'hybrid' scenario operation, where a broad low-shear q-profile with $q_{min} \sim 1$ is employed.

In principle, the shaping of the plasma can also affect the stability of the $n = 1$ internal kink mode. References [41, 60–62] show that typically smaller elongation and larger triangularity lead to increased internal kink mode stability. However, variations in elongation and triangularity of up to 10% have not yielded a change in the LLM behaviour. It thus appears that shaping is not a very effective control actuator in MAST because the range of triangularity accessible is not very wide, and the influence of the shape at r_1 is even smaller than at the last closed flux surface.

4. Role of fast ions

The fast ion fraction in high performance MAST plasmas can approach 0.3. At such high values the fast ions can play a strong role in determining the behaviour of MHD plasma instabilities. Indeed the stability of the LLM and its transition to/from fishbones are both strongly influenced by, and strongly influence, the fast ions. The interaction

between the internal kink mode and fast ions has been studied in much detail in recent years. It should be noted that whilst the fast ions will influence the stability of the LLM, they cannot be considered as a mechanism to cause the saturation of the kink mode since the presence of the LLM results in a redistribution of energetic particles, such that any stabilisation would be diminished allowing mode growth to occur.

4.1. Interaction between fast ions and the MHD unstable internal ideal mode

As well as increasing the plasma rotation resulting in gyroscopic stabilisation discussed in section 3.4, the NBI also introduces a population of fast ions which can affect the kink mode stability. There has been a great deal of analytical and numerical work in recent years devoted to the study of the internal kink mode in the presence of fast ions and rotation. This work was motivated by studying the influence of these actuators on sawtooth stability. It was found that the effects of the energetic ions result primarily from the top-hat internal kink mode eigenstructure and the inertial layer at the $q = 1$ surface. Although the hypothesis presented here suggests that the LLM becomes unstable without the presence of a $q = 1$ surface, the eigenstructure for strongly reversed shear q-profiles often present in MAST at LLM onset is still the same localised top-hat with an inertial layer at $r_1 = r(q_{min})$. Furthermore, the work concerning the sawtooth (de)stabilisation only considers an ideal kink mode, since the tearing at the rational surface is not thought to affect these stabilisation mechanisms. Consequently, it is appropriate to assume that similar stabilisation mechanisms will play a role in determining the onset of the LLM. It is however, important to reiterate that these mechanisms will only help to explain the linear stability thresholds and not the nonlinear saturation of the mode.

The trapped ions are typically have a strongly stabilising effect on the $n = 1$ internal kink mode [63], whilst the passing ions can be destabilising when injected outside the inertial layer position [33] or counter to the plasma current [37]. In a spherical tokamak, the trapped fraction is enhanced, and so the fast ions are dominantly stabilising. Their stabilisation effect can be altered by moving the deposition location [36], but even by doing this the overall effect is of significant stabilisation compared to Ohmic plasmas. Whilst it should be expected that the NBI fast ions will stabilise the internal kink which is unstable in strongly reversed shear plasmas, the good agreement between the ideal stability limits with respect to the Δq evolution and the experimental observation of LLM onset (as seen by comparing figure 1 with figure 12) suggests that fast ion stabilisation is a second order effect on mode stability.

It has also been shown analytically that the trapped energetic particles are stabilising [64] when inside r_1 for the weakly reversed shear q-profiles symptomatic of the final phase of MAST plasmas that exhibit the long lived mode [65]. Furthermore, Kolesnichenko et al [66, 67] have shown that the circulating ions inside r_1 stabilise the infernal mode as well. When $\beta_{hot} = 0.5\beta_{thermal}$, the maximum growth rate of the $n = 1$ infernal mode and the critical Δq at which the mode becomes unstable both reduce by

a factor of two. However, in MAST the fast ion β is not this high, and furthermore, the radial breadth of the region of low shear extends well beyond mid-radius, which diminished the effect of the energetic circulating ions [66]. It should be noted that the effect of the energetic passing particles is the same in conventional aspect ratio devices as in spherical tokamaks, so $\Delta q_{crit}(\beta_h = 0.5\beta) = 0.5\Delta q_{crit}(\beta_h = 0)$, which can be significant since $\Delta q_{crit}(\beta_h = 0)$ is much smaller in conventional aspect ratio devices.

Finally, it should be noted that work in reference [68] shows that the fast and thermal ions can drive internal instabilities. However, the change in the potential energy of the mode arising in the presence of energetic particles, δW_k, is significantly smaller than δW^{MHD} in MAST, where the ϵ^2 term in δW^{MHD} is much larger than would be the case in conventional aspect-ratio devices.

4.2. Ion diamagnetic effects

A well known effect which can dramatically modify stability of ideal MHD modes is the finite gyroradius effect of the ion diamagnetic frequency, which can stabilise ideal modes if their growth rate is lower or comparable to ω_{*i}. The ion diamagnetic frequency is defined as $\omega_{*i} = (neN)\mathrm{d}P_i/\mathrm{d}\psi \approx (m/rB)\mathrm{d}T/\mathrm{d}R$. It has been shown [69, 70] that ion diamagnetic effects can also strongly stabilise the internal kink mode. Indeed, such effects were invoked to explain the asymmetry in sawtooth behaviour between co- and counter-NBI heated plasmas in MAST [30]. Stronger diamagnetic stabilization could be expected at higher density, lower toroidal field (though this would come at the price of an increase in β) or for stronger pressure gradients. Menard et al [71] have suggested that diamagnetic stabilization in regions of low magnetic shear [72] could help to explain the saturated internal kink mode observed in NSTX. Finally it is worth noting that in regions where the ion diamagnetic frequency is large due to a strong pressure gradient, and a weakly-sheared or 'hybrid' q-profile is assumed, the plasma is likely to be unstable to infernal modes. It is possible to assess the role of the ion diamagnetism in stabilising the ideal internal modes observed in MAST by using the MISHKA-D code [70], which solves equations derived to extend the ideal one-fluid model to include the effect of ion diamagnetic drifts. Figure 19 illustrates the stabilising effect of ω_{*i} on both the internal kink mode found to be unstable in strongly reversed shear plasmas and the infernal mode found to be unstable in broad low-shear plasmas. As reported in reference [53], the growth rate of the $n = 1$ internal kink mode is steadily decreased as ω_{*i} increases until the mode is completely stabilised. In figure 19 the eigenvalues of the internal modes are found self-consistently by varying the parameter τ whilst keeping the pressure profile fixed, where

$$\omega_{*i} = \tau \frac{nq\langle|\nabla\psi|\rangle}{\rho_0\langle r\rangle\langle B_0\rangle}\frac{\mathrm{d}p}{\mathrm{d}\psi} \tag{12}$$

where $\langle\cdots\rangle$ represents an averaging over a flux surface and ρ_0, B_0 are the equilibrium mass density and magnetic field respectively. Whilst increasing ion diamagnetic frequency can completely stabilise the internal kink mode (though not at typical MAST

values, increasing ω_{*i} does not fully suppress the infernal mode. This behavior is related to the large variation of ω_{*i} at the rational surfaces arising from radial variation in the pressure gradient. As explored in reference [70], complete stabilisation could, in principle, be obtained when the density profile balances the radial change in the pressure gradient such that ω_{*i} is relatively constant as a function of radius. However, including the ion diamagnetic effects on the infernal mode only has a small effect on the beta for required for marginal stability, consistent with the appearance of the LLM being well predicted by the calculated ideal MHD stability limits.

Whilst there is no $q = 1$ rational surface in these MAST advanced tokamak scenario plasmas, there are of course rational surfaces at $q = 2$, $q = 3$ etc. Consequently, islands could be anticipated to form at these radial locations when the LLM occurs in the plasma. However, no such islands are observed on the soft X-ray or Thomson scattering diagnostic measurements. This could be explained by the strong flow shears present in MAST, or from the large ion diamagnetic frequency, both of which are stabilising to higher-(m, n) resistive harmonics.

4.3. Fishbones and fast ion losses

As the current diffuses into the core and the safety factor evolves downwards, MAST plasmas usually experience a phase of $n = 1$ fishbone activity before the LLM appears, as illustrated in figure 1. The dispersion relation for fishbones with a monotonic q-profile and a $q = 1$ surface was derived in reference [73] as

$$-i\frac{\omega}{\tilde{\omega_A}} + \delta\hat{W}_f + \delta\hat{W}_k \tag{13}$$

where $\tilde{\omega_A} = \omega_A/\sqrt{3}s_1$, $\delta\hat{W}_f = 2R_0\delta W^{MHD}/\pi r_1^2 B_0^2|\xi_0|^2$ and $\delta\hat{W}_k$ is the change in the potential energy of the internal kink mode due to the presence of trapped energetic ions. By substituting into δW_k a slowing down distribution, $F_{0h} = c_0 E^{-3/2}\delta(\lambda - \lambda_0)$ where $c_0(r)$ is defined in reference [73], and substituting in equation 1 [38] such that

$$\gamma/\omega_A s_1 + \delta\hat{W}_f \rightarrow \sqrt{r_1 q''}\bar{\gamma}^{3/2}\Big[1 + \frac{\Delta q}{\bar{\gamma}}\Big]^{1/2} + \delta\hat{W}_f \tag{14}$$

means that equation 13 is transformed into the dispersion relation for fishbones in equilibria with non-monotonic q-profiles as

$$\delta\hat{W}_f + \sqrt{r_1^2 q''}\Big[(\Delta q)^2 - 3\Omega(\Omega - \Omega_{*pe})\Big(\frac{\bar{\omega}_{dm}^2}{\omega_A^2}\Big)\Big]^{1/2}\Big[\Delta q + \Big((\Delta q)^2 - 3\Omega(\Omega - \Omega_{*pe})\frac{\bar{\omega}_{dm}^2}{\omega_A^2}\Big)^{1/2}\Big]^{1/2} + \langle\beta_h\hat{I}_0\rangle\Omega\log\Big(1 - \frac{1}{\Omega}\Big) = 0 \tag{15}$$

where $\Omega = \omega/\bar{\omega_{dm}}$, $\bar{\omega}_{dm} = \bar{\omega_{dh}}(E = E_m)$, $\bar{\omega}_{dh}$ is the toroidal precession frequency of the trapped energetic particles, E_m is the upper bound of the energy range of the fast ion distribution, β_h is the fast ion beta and $\hat{I}_0$ is defined in reference [73]. For fishbones to be unstable in plasmas with a monotonic q-profile, the β_h term must be sufficiently large as to overcome the Alfvén continuum damping around the $q = 1$ surface. However, in reversed shear plasmas, the continuum damping can be eliminated without the ω_{*pi}

diamagnetic terms to produce a continuum gap. Indeed if $\Delta q > 0$, the continuum gap is in the range $[-\Delta q\omega_A/\sqrt{3}, +\Delta q\omega_A/\sqrt{3}]$. Since the $\delta\hat{W}_f$ term in equation 15 is negative for a non-monotonic q-profile (for sufficiently large Δq), the fishbones can be driven unstable at a much lower value of β_h than in a plasma with a monotonic q-profile and positive $\delta\hat{W}_f$.

It is also possible to compare the Δq required in a reversed shear plasma to drive fishbones compared to that required for the ideal internal mode to become unstable. Analytically, we have found that the fishbones are unstable at a much higher Δq than the ideal mode. Using the drift kinetic HAGIS code [74], it is possible to simulate a fishbone mode when $\Delta q > \Delta q_{crit}$. When the internal eigenfunction is supplied to HAGIS and the wave is evolved in the presence of a typical fast ion distribution, it is found that the kinetic drive is greater than the damping of the mode, and consequently the plasma would be unstable to fishbones. The fact that fishbones would be unstable at a larger Δq than required for the LLM to become unstable agrees well with the behaviour exhibited experimentally as the safety factor evolves. Once $\Delta q < \Delta q_{crit}$ and the LLM is born in the plasma, the enhanced fast ion losses associated with the mode means that there are no longer sufficient energetic ions within the core of the plasma to drive the fishbones, and the chirping activity ceases. A detailed analysis of fishbones in reversed shear plasmas and the transition from the fishbone phase to a saturated ideal mode will be discussed in more details in a future publication [75].

When the plasma is subject to the saturated displacement of the core, the fast ion losses are enhanced, as exemplified by figure 4. This occurs when the energetic ions born in the plasma due to the neutral beam heating are displaced sufficiently far that their large drift orbits then traverse the last closed flux surface, and are lost from the plasma. In spherical tokamaks like MAST the trapped fraction of the fast particles is larger than in conventional aspect ratio devices (the trapped-passing boundary is at $v_\parallel/v = \sqrt{2r/[R_0 + r]}$), and their orbit widths are large compared to the minor radius of the plasma. Furthermore, the radial location of the minimum in the safety factor is typically beyond the mid-radius of the plasma, and consequently the radial displacement of the core plasmas will also encompass a significant volume of the plasma core since the mode eigenfunction extends to r_1. Consequently, the kink displacement results in far more lost fast ions in spherical tokamak plasmas than would be expected in conventional aspect-ratio plasmas.

5. Rotation damping

When the LLM appears in MAST plasmas, a strong damping of core rotation is measured by the charge exchange diagnostic (see figure 3). The short time scale of this process (∼10ms) compared to MAST confinement times (∼50ms) excludes MHD-induced momentum transport as a cause for the plasma braking. Fast Thomson scattering temperature profiles and relative phases of different soft X-ray channels show no evidence of the presence of magnetic islands, which rules out electromagnetic torques

associated with resistive effects at resonant layers. Moreover, these torques are strongly localised, inconsistent with a simultaneous slowing down of the entire plasma core. In contrast, the non-resonant instantaneous distributed torque predicted by Neoclassical Toroidal Viscosity (NTV) [76] seems well suited to describe the measured braking of the plasma by this MHD mode. The torque predicted by NTV has been compared with experimental observations. The structure of the long-lived mode is first determined using the CASTOR linear code [49] with zero resistivity, a setting justified by the absence of any island in the plasma, and its saturated amplitude is estimated by comparing results of the forward analysis of the soft X-ray emission to experimental data, as described in section 3.5 and reference [56]. Based on this information, the NTV torque is calculated and compared to experimental data.

NTV theory has been extensively applied to externally-driven, static, magnetic perturbation cases [77]. This theory can also be used if the field's asymmetry is broken by the presence of an MHD instability [71], in which case the torque arises from the differential flow of the plasma through the non-axisymmetric perturbation. The flow considered here is the motion of the ion fluid, the velocity of which is assumed to be equal to that of the carbon fluid measured by charge exchange spectroscopy. An intuitive understanding of the slowing down process is as follows: The mode's structure can only remain coherent if it rotates as a rigid body, while single-fluid MHD theory prescribes the plasma, despite its sheared rotation, to be frozen in the magnetic field. In effect, multi-fluid MHD equations allow the motion of the magnetic field lines to depart from that of the fluid. This shift is of the order of the diamagnetic frequency, and results in a less strict, shifted, frozen-in condition. These two competing velocity profiles are equilibrated during a transition phase, viz the slowing down of the plasma. In a collisional plasma, this is because the fluid contracts and expands as it goes through the distorted flux surfaces, thus leading to viscous dissipation in a mechanism similar to magnetic pumping. In the collisionless case, the orbit of banana-trapped particles drifts radially, creating a radial current which acts on the flow by generating a $\vec{j} \times \vec{B}$ torque.

The angular frequency profiles of the plasma in MAST discharge 21781 during the braking phase are shown in figure 3. The rotation is unchanged for the radial location R=1.15m. It is tempting to interpret this point as the position where the mode's frequency and that of plasma are equal, hence where one would expect the torque applied by the mode to vanish. In effect, this is not the case. The mode frequency in MAST shot 21781 is 20kHz at the time of LLM onset whereas the frequency of the point of inversion is 14kHz. This can be explained, in an intuitive manner, by the shifted frozen-in condition mentioned earlier, or, in a mathematical way, by the presence of the offset velocity ω^*_{NC} in the NTV formulation [76]. Incidentally, these two shifts are of the order of the diamagnetic frequency, and so is the difference in frequency between the mode and the point of unchanged rotation. The torque predicted by NTV is shown in figure 20, together with the measured rate of change of angular momentum for each flux tube. The prediction and observation have the same order of magnitude. The profile shapes are similar, except in the vicinity of the rational surfaces and the inertial layer. There,

large parallel magnetic field perturbations result in a high torque which is not observed experimentally. The disagreement is probably due to the fact that the linear structure used here is likely to differ from the saturated eigenstructure in these regions. The large number of plasma profiles involved in this calculation means that uncertainties are difficult to assess and may be large. These do not compromise the results presented here, but they do prohibit more detailed comparison. It is however worth mentioning that the inclusion of the offset velocity ω^*_{NC} is crucial in order to reproduce the measured torque profile with NTV theory. Furthermore, the Lagrangian term $(\xi\cdot\nabla)B_0$ must be taken into account to predict a torque of magnitude comparable to that observed experimentally, its absence decreasing the calculated result by approximately 70%. Thus, the plasma braking predicted by NTV theory is consistent with the observed damping of core rotation due to the presence of the LLM.

It is likely that there are also other contributory factors to the rotation damping observed in the presence of the LLM. For instance, the fast ion redistribution cause by the displacement of the plasma core will incur a momentum transport, resulting in a slowing down of the core plasma.

6. Discussion and conclusions

In order to optimise the plasma performance and minimise the cost of electricity, the plasma in a future fusion power plant must operate with high β and, simultaneously, a large fraction of bootstrap current to minimise the power requirements from auxiliary heating systems. Plasma current profiles in largely bootstrap current driven equilibria are generally broad resulting in reversed shear or low-shear safety factor profiles. However, the strong pressure gradients required for optimal fusion performance combined with these q-profiles can result in deleterious MHD instabilities. Recent MAST discharges have investigated plasma stability in advanced tokamak regimes as the q-profile naturally transitions from strongly reversed shear to a very broad low-shear region with $q_{min} \sim 1$. Saturated internal modes are found to occur when Δq becomes small enough, resulting in a strong braking of the core plasma, enhanced fast ion losses and degradation of the energy confinement. This has significant implications for the operation of advanced tokamak regimes, both in future spherical tokamaks, and conventional aspect-ratio devices.

Similar saturated mode appearance has been reported in high performance NSTX discharges which had similar reversed shear q-profiles with $q_{min} \sim 1$ [78, 79]. However, in reference [71], the saturated internal modes are found to be resistive modes where islands are observed. The saturation of these resistive instabilities is described in terms of ion diamagnetic effects and two-fluid effects, after rotation and fast ion stabilisation had been discounted on the grounds that the saturated modes result in fast ion losses and plasma braking, similar to the phenomena observed in MAST. The saturation of the LLM in MAST is due to the ideal nature of the instability. At a sufficiently large amplitude of the displacement, the stabilising field-line bending term in the ideal MHD

equations will dominate and prevent further growth – naturally this would not be the case if an island were present. Furthermore, the plasma braking was attributed to the electromagnetic torque arising in the presence of the magnetic island [71], again in contradiction to the results observed here, where no magnetic islands are observed and the braking is attributed to neoclassical toroidal viscosity effects and fast ion losses.

The LLM occurs in MAST plasmas with the safety factor above unity and there are no indications of magnetic reconnection. Consequently, the internal kink modes and infernal modes which are driven unstable in strongly reversed shear plasmas and broad low-shear plasmas respectively, should be anticipated when Δq is sufficiently small. This sets a limit on how close the safety factor can approach the rational surface before these MHD instabilities are driven unstable. Whilst the presence of energetic ions, strong plasma rotation and the ion diamagnetic frequency all play a stabilising role and could help to delay these ideal modes, at sufficiently high plasma β (as required in advanced tokamaks for economically attractive fusion performance) the ideal MHD drive will result in plasma instabilities. This could offer a possible explanation for behaviour recently observed in various conventional aspect ratio devices. In advanced tokamak regimes in JET, either with a broad low-shear region and $q_{min} \sim 1$ or with reversed shear and $q_{min} \sim 2$, ideal $m/n = 2/1$ modes are driven unstable and exist in a saturated state for some time, before they transition into tearing mode [80, 81]. These so-called 'continuous' modes follow a period of fast-ion driven chirping modes and result in rotation flattening in the core and substantial reduction in performance, analogous to the LLM observed in MAST. One explanation of this behaviour could be that infernal modes driven by strong pressure gradients become unstable as Δq becomes sufficiently small. This is supported by the comparison of high-field side and low-field side magnetic signals which suggest that these modes have a kink-ballooning structure [81]. In JET, the large suprathermal pressure fraction, which typically approaches one third, means that Δq_{crit} could be expected to be somewhat smaller than that predicted by ideal MHD. Nonetheless, the slow evolution of q towards the rational surface allows the ideal mode to become unstable before q_{min} crosses the rational value and magnetic tearing becomes energetically favourable. Similar observation of slowly-growing ideal modes has been reported in both JT-60U [82] and DIII-D [83].

One of the primary benefits of advanced scenarios is that they deliberately avoid the introduction of low-q rational surfaces, which precludes various detrimental resistive instabilities, such as low-(m, n) neoclassical tearing modes and sawteeth. However, it is clear that as well as avoiding these resistive instabilities by keeping q_{min} above the relevant rational surface, it is important to keep Δq sufficiently large as to avoid ideal instabilities too. This is particularly pertinent to the 'hybrid' scenario – proposed as a possible high-Q regime for ITER operation – since it is anticipated to have a broad low-shear region with $q_{min} \sim 1$. The ramifications of destabilisation of such ideal internal modes in ITER could be heightened, as islands should be anticipated at higher rational surfaces since the flow shear is unlikely to be sufficiently strong to suppress these higher-(m, n) resistive harmonics as is the case in MAST. Modelling to assess advanced scenario

stability in ITER will be the subject of future investigation.

Whilst there is a need to develop advanced tokamak scenarios for ITER which keep Δq sufficiently large to avoid ideal instabilities, spherical tokamaks are even more susceptible to such ideal internal modes. The inverse aspect-ratio scaling evident in the expression for Δq_{crit} means that the internal kink mode and the infernal mode are unstable at a significantly larger Δq in spherical tokamaks than in conventional aspect-ratio devices. Consequently, the ultimate goal of high performance spherical tokamaks, such as a components test facility (ST-CTF) [57] must be to keep the safety factor well above the rational surface with a large fraction of non-inductive current drive and thereby avoid these performance limiting ideal internal modes. Indeed, NSTX operation with the safety factor well above unity has contributed to significantly improving plasma performance and lengthening pulse duration [84].

Acknowledgements

The authors would like to acknowledge useful discussions with Dr N Arcis and Dr SE Sharapov. This work was partly funded by the United Kingdom Engineering and Physical Sciences Research Council, the Écold Polytechnique (Palaiseau, France), the British Council and by the European Communities under the contract of Association between EURATOM and UKAEA and the Fonds National Suisse de la Recherche Scientifique. The views and opinions expressed herein do not necessarily reflect those of the European Commission.

References

[1] Becoulet A and Hoang GT, 2008 *Plasma Phys. Control. Fusion* **50** 124055
[2] Litaudon X et al, 2007 *Plasma Phys. Control. Fusion* **49** B529
[3] Joffrin E, 2007 *Plasma Phys. Control. Fusion* **49** B629
[4] Doyle EJ et al, 2006 *Plasma Phys. Control. Fusion* **48** B39
[5] Taylor TS 1997 *Plasma Phys. Control. Fusion* **39** B47
[6] Bickerton RJ et al, 1971 *Nat. Phys. Sci.* **229** 110
[7] Manickam J et al, 1994 *Phys. Plasmas* **1** 1601
[8] Huysmans GTA, Hender TC, Hawkes N and Litaudon X, 2001 *Phys. Rev. Lett.* **87** 245002
[9] Sips ACC et al, 2005 *Plasma Phys. Control. Fusion* **47** A19
[10] Joffrin E, 2005 *Nucl. Fusion* **45** 626
[11] Strait EJ *et al* 1995 *Phys. Rev. Lett.* **74** 2483
[12] Hender TC *et al* 2006 *21st IAEA Fusion Energy Conference, Chengdu, China* **EX/P8-18**
[13] Sabbagh SA *et al* 2006 *Nucl. Fusion* **46** 635
[14] Garofalo AM *et al* 2002 *Phys. Plasmas* **9** 1997
[15] La Haye RJ *et al* 2004 *Nucl. Fusion* **44** 1197
[16] Sontag AC *et al* 2005 *Phys. Plasmas* **12** 056112
[17] Reimerdes H *et al* 2007 *Phys. Rev. Lett.* **98** 055001
[18] Takechi M *et al* 2007 *Phys. Rev. Lett.* **98** 055002
[19] Strait EJ *et al* 2007 *Phys. Plasmas* **14** 056101
[20] Sabbagh SA *et al* 2008 *22nd IAEA Fusion Energy Conference, Geneva, Switzerland* **EX/5-1**
[21] Chapman IT *et al* 2009 *Plasma Phys. Control. Fusion* **51** 055015
[22] Liu YQ et al, 2009 *Phys. Plasmas* **16** 056113
[23] Liu YQ et al, 2008 *Phys. Plasmas* **15** 092505

[24] Challis C et al 2009 *36th EPS Conference on Plasma Physics* O5.057
[25] de Bock MFM et al, 2009 *36th EPS Conference on Plasma Physics, Sofia* P5.186
[26] Meyer HF et al, 2009 *to appear in Nucl. Fusion*
[27] Budny R *et al* 1992 *Nucl. Fusion* **32** 429
[28] Gryaznevich MP et al, 2008 *Nucl. Fusion* **48** 084003
[29] Lao L et al, 1990 *Nucl. Fusion* **30** 1035
[30] Chapman IT et al, 2006 *Nucl. Fusion* **46** 1009
[31] Chapman IT et al, 2007 *Plasma Phys. Control. Fusion* **49** B385
[32] Turnyanskiy MR et al, 2009 *Nucl. Fusion* **49** 065002
[33] Graves JP, 2004 *Phys. Rev. Lett.* **92** 185003
[34] Chapman IT et al, 2009 *Nucl. Fusion* **49** 035006
[35] Chapman IT et al, 2008 *Plasma Phys. Control. Fusion* **50** 045006
[36] Chapman IT et al, 2009 *Phys. Plasmas* **16** 072506
[37] Chapman IT et al, 2007 *Phys. Plasmas* **14** 070703
[38] Hastie RJ et al, 1987 *Phys. Fluids* **30** 1756
[39] Bussac MN et al, 1975 *Phys. Rev. Lett.* **35** 1638
[40] Avinash et al, 1987 *Phys. Rev. Lett.* **59** 2647
[41] Holmes JA et al, 1988 *Phys. Fluids* **31** 1202
[42] Luce TC et al, 2003 *Nucl. Fusion* **43** 321
[43] Hastie RJ and Hender TC, 1988 *Nucl. Fusion* **28** 585
[44] Waelbroeck FL and Hazeltine RD, 1988 *Phys. Fluids* **31** 1217
[45] Wahlberg C and Graves JP, 2007 *Phys. Plasmas* **14** 110703
[46] Graves JP 2009 *Private Communication*
[47] Wahlberg C and Graves JP, 2007 *12th European Fusion Theory Conference, Madrid*
[48] Huysmans G, Goedbloed J and Kerner W 1991 *Proceedings of the CP90 Conference on Computer Physics*, (World Scientific, Singapore), p. 371
[49] Kerner W et al, 1991 *Contr. Fusion and Plas. Phys. 18th Conf. Berlin* Part IV, p89
[50] Mikhailovskii AB, Huysmans GTA, Sharapov SE and Kerner WO 1997 *Plasma Phys. Rep.* **23** 844
[51] Waelbroeck FL, 1996 *Phys. Plasmas* **3** 1047
[52] Wahlberg C and Bondeson A, 2000 *Phys. Plasmas* **7** 923
[53] Chapman IT *et al* 2006 *Phys. Plasmas* **13** 062511
[54] Wahlberg C, Chapman IT and Graves JP 2009 *sub Phys. Plasmas*
[55] Chapman IT, Graves JP and Wahlberg C, 2009 *sub Nucl. Fusion*
[56] Hua M-D, Chapman IT, Field AR, Pinches SD and Garzotti L 2009 *sub Plasma Phys. Control. Fusion*
[57] Wilson HR *et al* 2004 *20th IAEA Fusion Energy Conference, Villamoura* FT/3-1Ra
[58] Morris AW *et al* 2005 *Fusion Engineering and Design* **75** 67
[59] Peng Y-K M *et al* 2005 *Plasma Phys. Control. Fusion* **47** B263
[60] Connor JW and Hastie RJ, 1985 *Internal Report CLM-M-106* "The effect of shaped plasma cross sections on the ideal internal kink mode in a tokamak"
[61] Lutjens H, Bondeson A and Vlad G, 1992 *Nucl. Fusion* **32** 1625
[62] Martynov A, Graves JP and Sauter O, 2005 *Plasma Phys. Control. Fusion* **47** 1743
[63] Porcelli F, 1991 *Plasma Phys. Control. Fusion* **33** 1601
[64] Helander P et al, 1997 *Phys. Plasmas* **4** 2181
[65] Gimblett CG et al, 1996 *Phys. Plasmas* **3** 3369
[66] Kolesnichenko YI, Lutsenko VV, Marchenko VS and White RB, 2007 *Phys. Plasmas* **14** 012504
[67] Kolesnichenko YI et al, 2007 *Plasma Phys. Control. Fusion* **49** A159
[68] Zonca F et al, 1999 *Phys. Plasmas* **6** 1917
[69] Hastie RJ, Catto PJ and Ramos JJ, 2000 *Phys. Plasmas* **7** 4561
[70] Huysmans GTA et al, 2001 *Phys. Plasmas* **8** 4292
[71] Menard JE et al, 2005 *Nucl. Fusion* **45** 539

[72] Rogers B and Zakharov L, 1995 *Phys. Plasmas* **2** 3420
[73] Chen L, White RB and Rosenbluth MN, 1984 *Phys. Rev. Lett.* **52** 1122
[74] Pinches SD et al, 1998 *Comput. Phys. Commun.* **111** 133 (Release Version 8.08)
[75] Pinches SD et al, 2009 *in preparation*
[76] Shaing KC et al, 2003 *Phys. Plasmas* **10** 1443
[77] Cole AJ et al, 2007 *Phys. Rev. Lett.* **99** 1065001
[78] Sabbagh SA et al, 2002 *Phys. Plasmas* **9** 2085
[79] Menard JE et al, 2003 *Nucl. Fusion* **43** 330
[80] Buratti P et al, 2008 *35th EPS Conference on Plasma Physics, Crete* P1.069
[81] Buratti P et al, 2009 *36th EPS Conference on Plasma Physics, Sofia* O2.007
[82] Matsunaga G et al, 2008 *22nd IAEA Fusion Energy Conference, Geneva* EX/5-2
[83] Okabayashi M et al, 2008 *22nd IAEA Fusion Energy Conference, Geneva* EX/P9-5
[84] Menard JE et al, 2007 *Nucl. Fusion* **47** S645

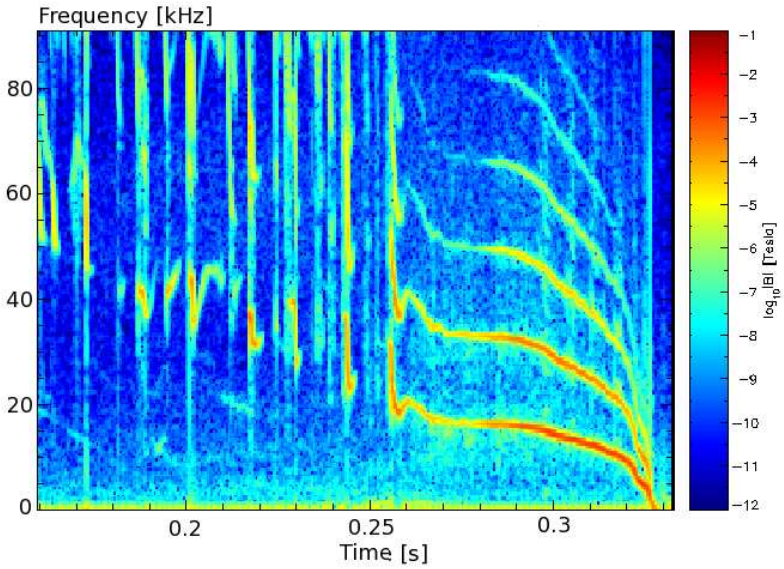

Figure 1. Fourier spectrogram of outboard midplane magnetic probe measurements in MAST discharge 21781. The chirping modes which transition to a long-lived saturated mode are typical of MAST neutral beam heated plasmas.

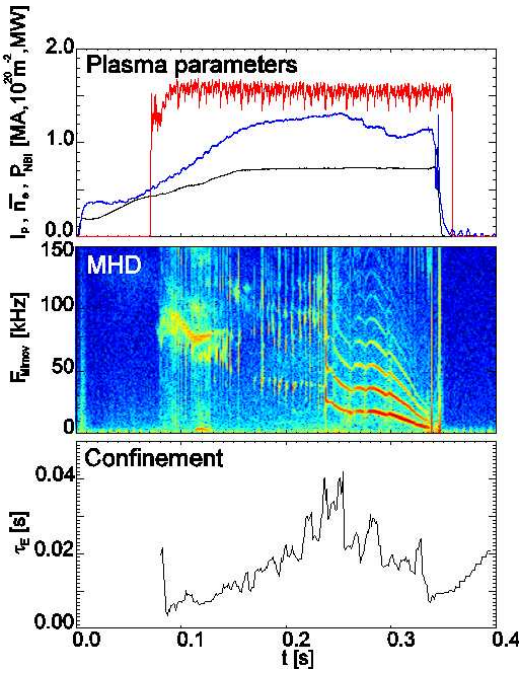

Figure 2. The plasma current, density and NBI power; the magnetic spectrogram; and the energy confinement time predicted by TRANSP for MAST shot 17661. The confinement time drops significantly after the LLM onset as the anomalous fast ion diffusion rate is increased in order to match the increased neutron rate observed experimentally.

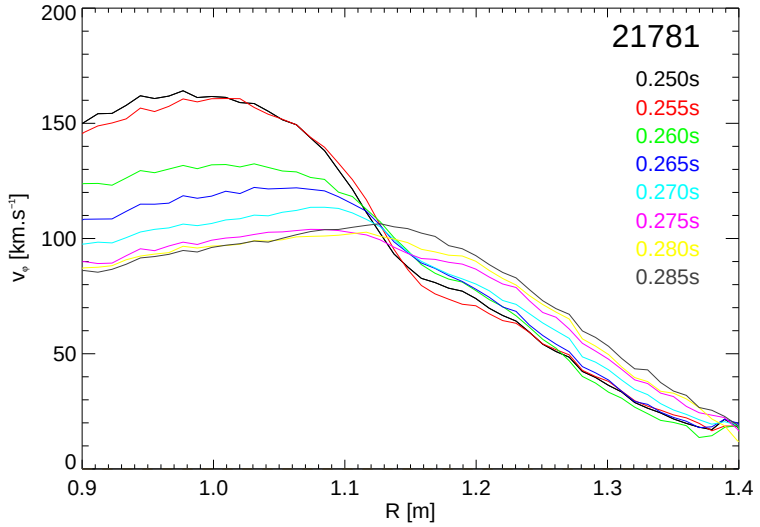

Figure 3. The rotation profiles measured by charge exchange recombination spectroscopy for MAST shot 21781 at a series of time points. The LLM onset, as illustrated in figure 1, is at 255ms.

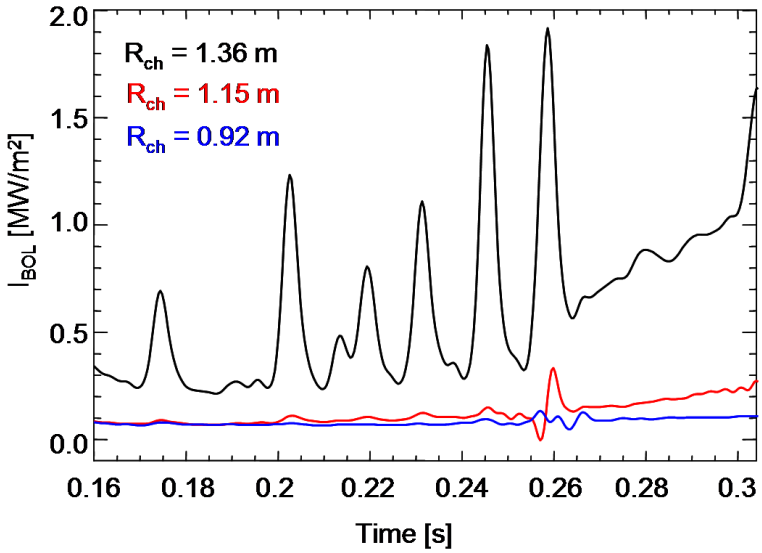

Figure 4. Fast ion losses seen by the counter-viewing bolometer during MAST discharge 21781. A peak in the fast ion losses from the edge channel is seen at each fishbone chirp, and the loss rate increases steadily after LLM onset (255ms), even as measured by channels further towards the plasma core.

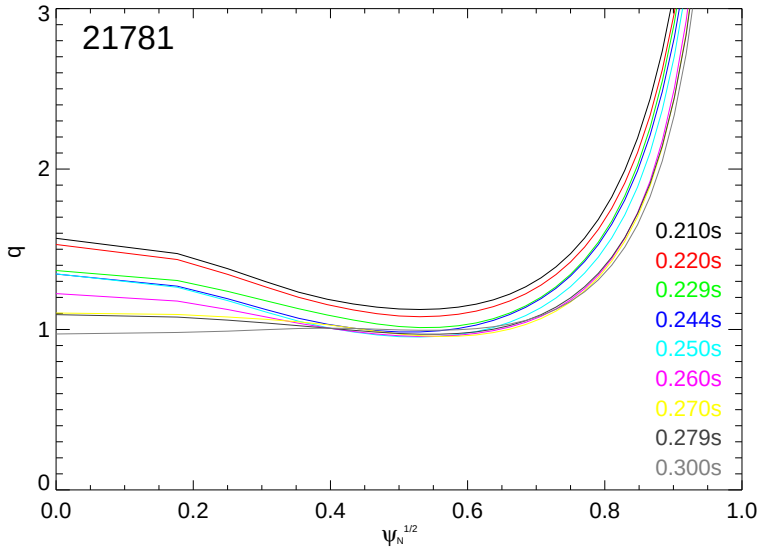

Figure 5. The q-profile as determined by the EFIT code constrained by the MSE measurements for MAST shot 21781 at a series of time slices.

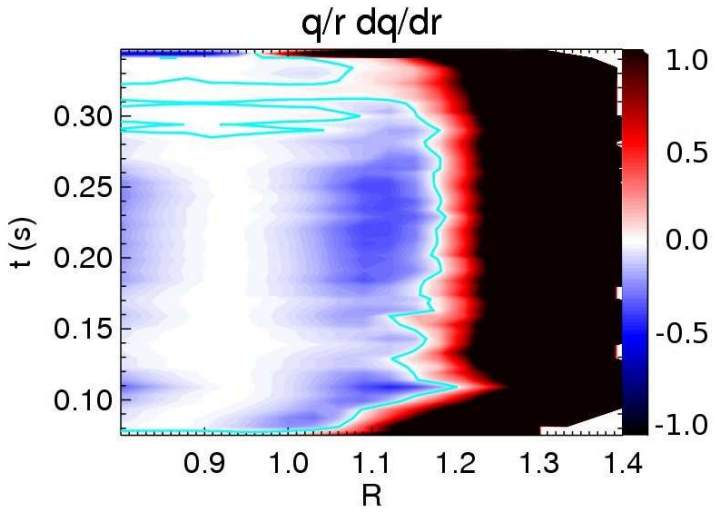

Figure 6. The magnetic shear for MAST discharge 21781 as a function of time and major radius. It is clear that the profile is either reversed shear, or flat at all times during the q-profile evolution.

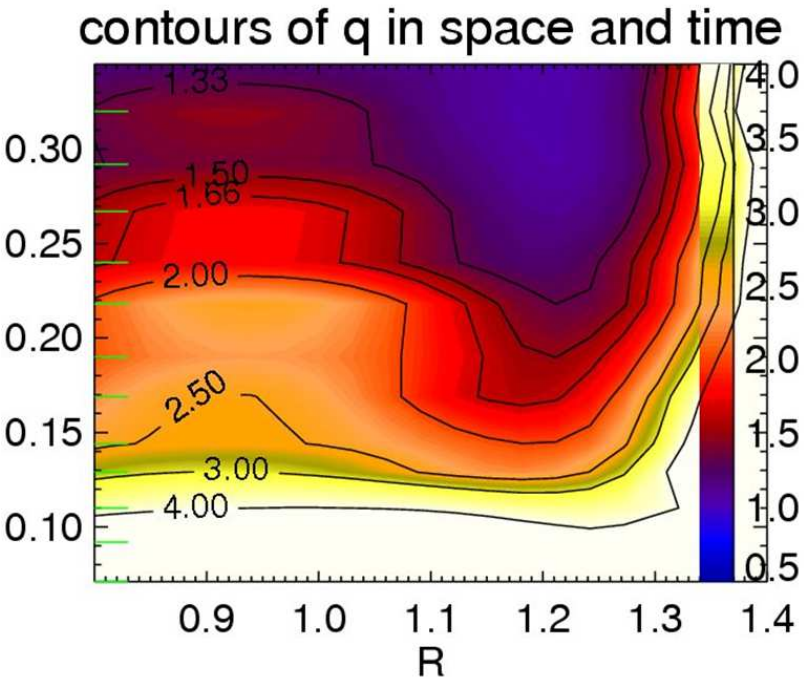

Figure 7. The q-profile for MAST discharge 22131 as a function of radius and time. The profile evolves from strongly reversed sheared to very broad and flat, but always with $q > 1$.

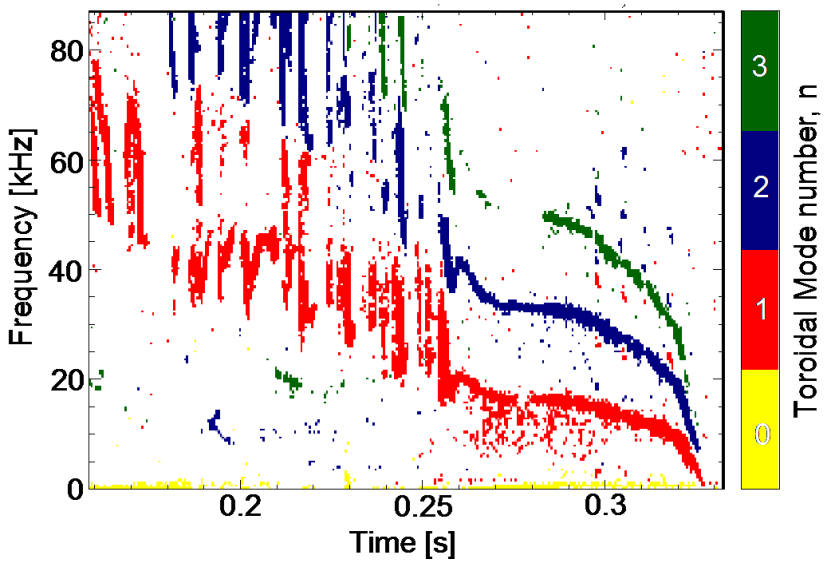

Figure 8. The toroidal mode number spectrogram for discharge 21781 as found from Fourier transform of the magnetic probe measurements at the midplane.

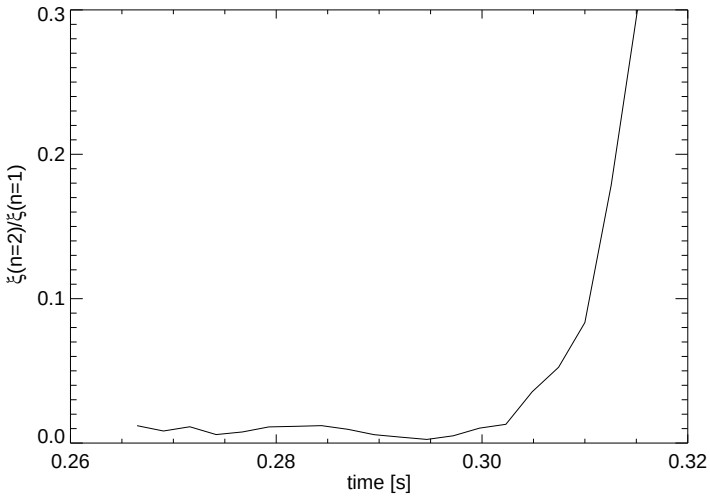

Figure 9. The amplitude of the $n = 2$ mode with respect to the $n = 1$ mode as found from the soft X-ray emission as a function of time.

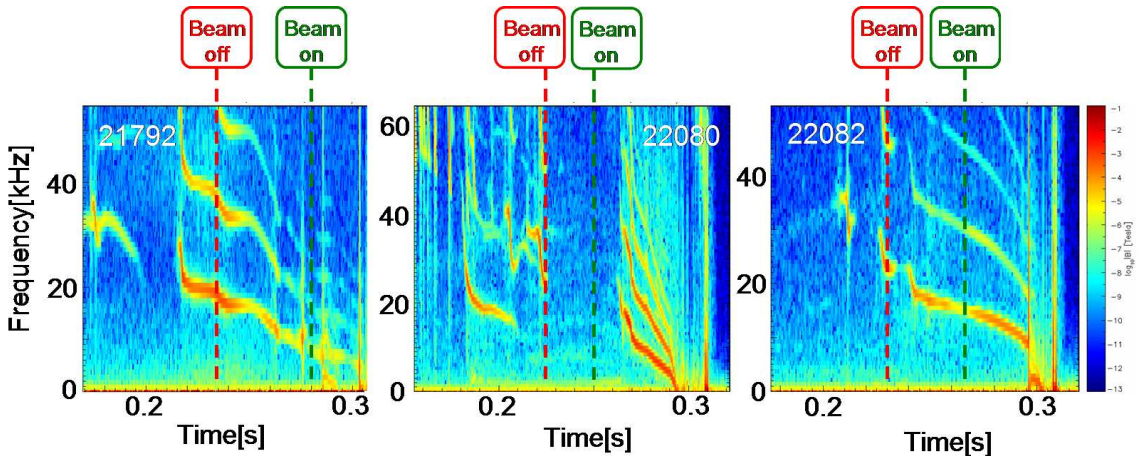

Figure 10. LLM behaviour in three similar MAST shots with slightly different neutral beam heating waveforms. In discharge 21792 the NBI window allows the safety factor to evolve below one, so sawteeth occur before the beam is reapplied. In 22080 the beam window is too short to allow q to evolve below one, so the LLM appears after the second beam is applied and β increases sufficiently. In 22082, the LLM appears during the window and is sustained by the second beam keeping $q > 1$.

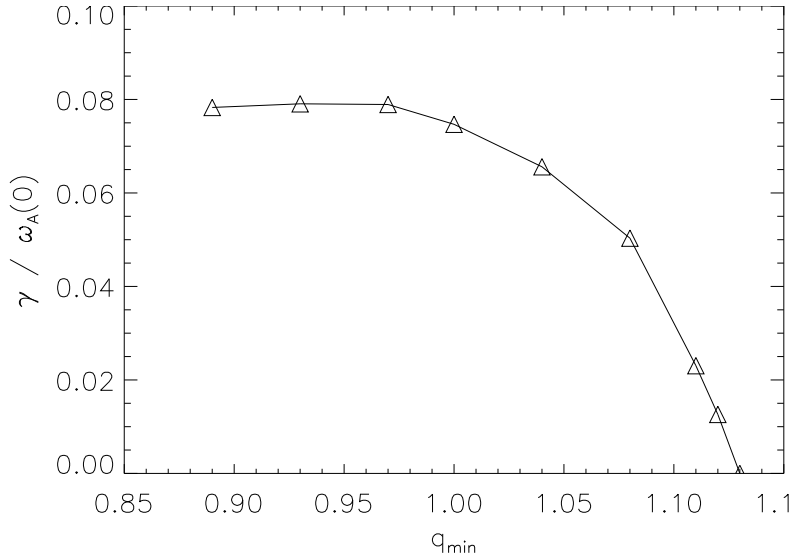

Figure 11. The growth rate of the internal $n = 1$ modes as a function of Δq for MAST shot 21508. The q-profile is taken at the time of the LLM onset and then scaled by varying the toroidal field, so that the q-profile shape remains constant as q_{min} changes.

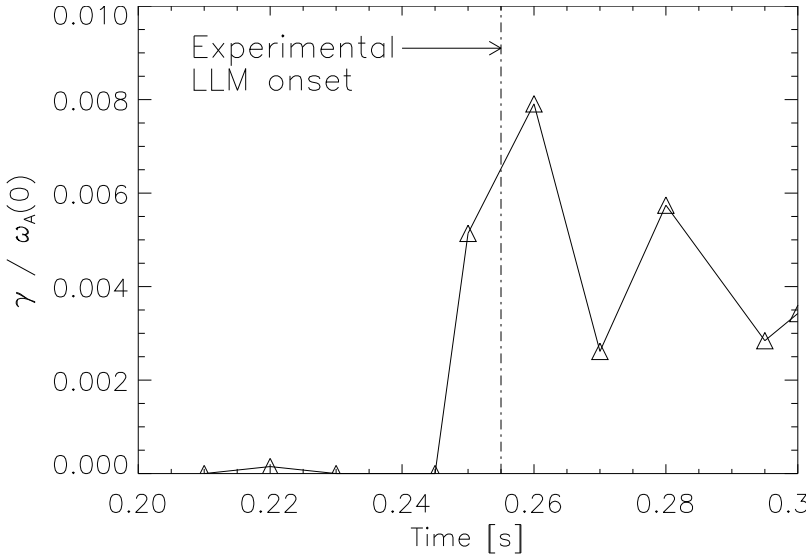

Figure 12. The growth rate of the internal $n = 1$ modes as a function of time for MAST shot 21781. The equilibria at each time slice are reconstructed using the MSE diagnostic measurements. The mode becomes ideally unstable at approximately the same time as it appears in the plasma, indicating that to first order, the ideal fluid drive appears to determine the point of marginal stability.

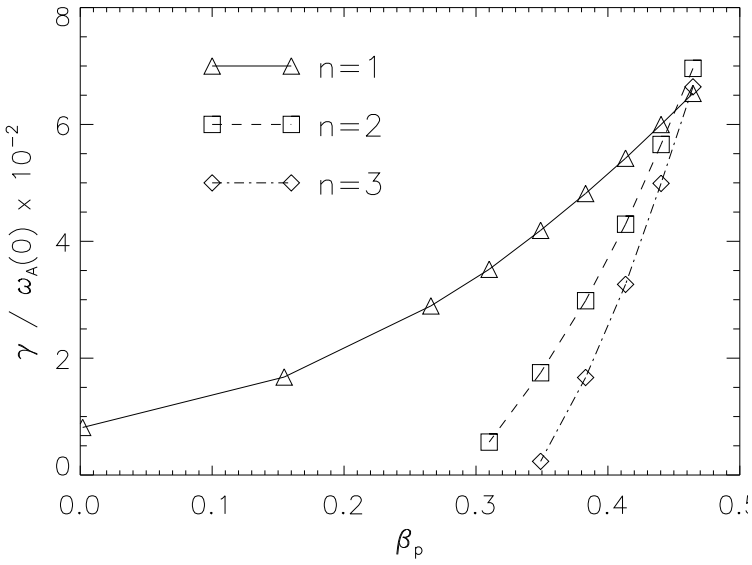

Figure 13. The growth rate of the $n = 1$, $n = 2$ and $n = 3$ ideal modes as a function of β_p for $\Delta q = 0.02$ for MAST discharge 21781.

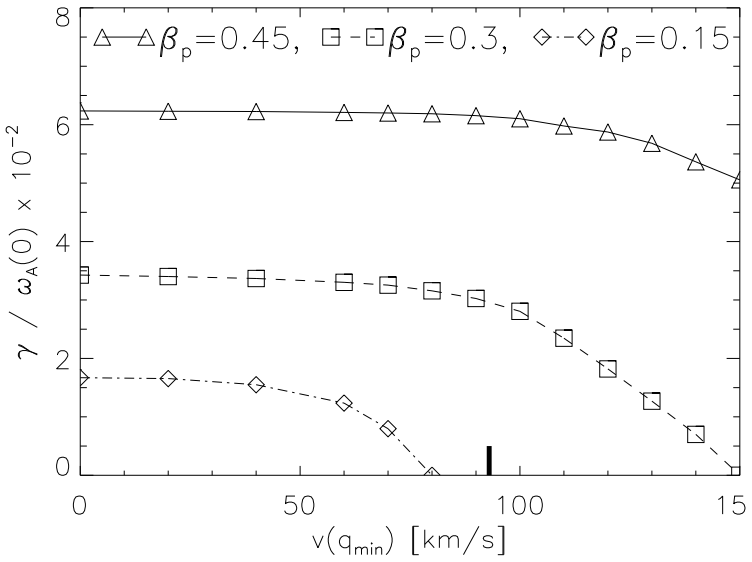

Figure 14. The growth rate of the $n = 1$ internal mode as a function of toroidal rotation at the radial location of q_{min} for different β_p. For comparison, the experimental level of the rotation at the time of LLM onset is marked by the tick mark on the x-axis.

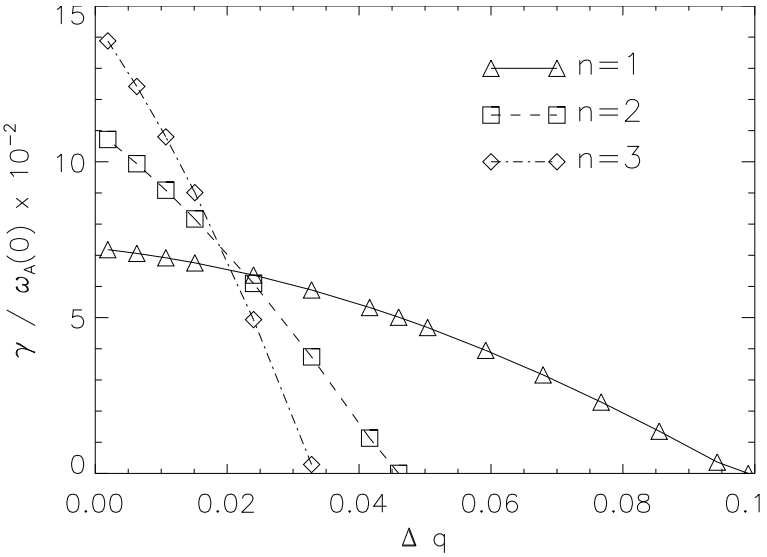

Figure 15. The growth rate of the internal $n = 1$, $n = 2$ and $n = 3$ modes as a function of Δq for MAST shot 21781. The q-profile is taken at the time of the LLM onset and then scaled by varying the toroidal field, so that the shape of the q-profile remains constant as q_{min} changes.

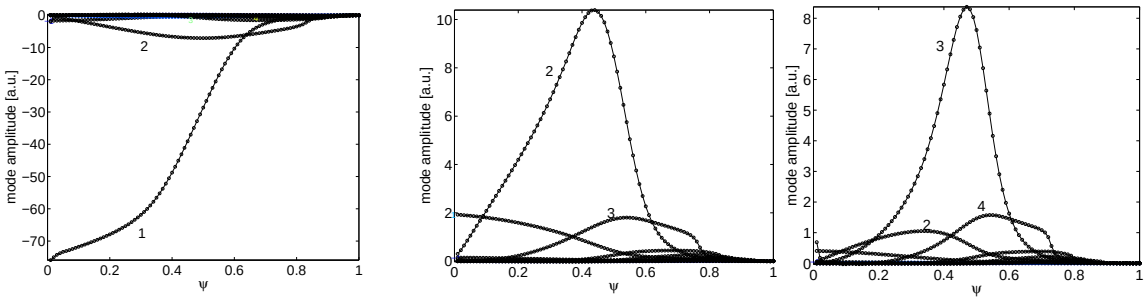

Figure 16. The eigenfunction of the $n = 1$, $n = 2$ and $n = 3$ ideal modes found unstable at $\Delta q = 0.02$ for MAST shot 21781, illustrating the infernal mode structure present with a broad low-shear region.

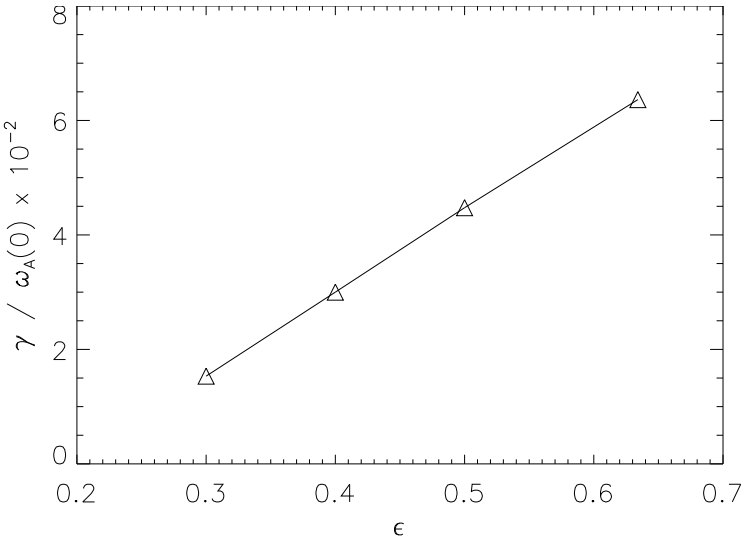

Figure 17. The growth rate of the $n = 1$ ideal mode as a function of the inverse aspect ratio at constant β (and consequently, varying Δq). It is clear that the $n = 1$ internal mode is more unstable for tight aspect ratio plasmas.

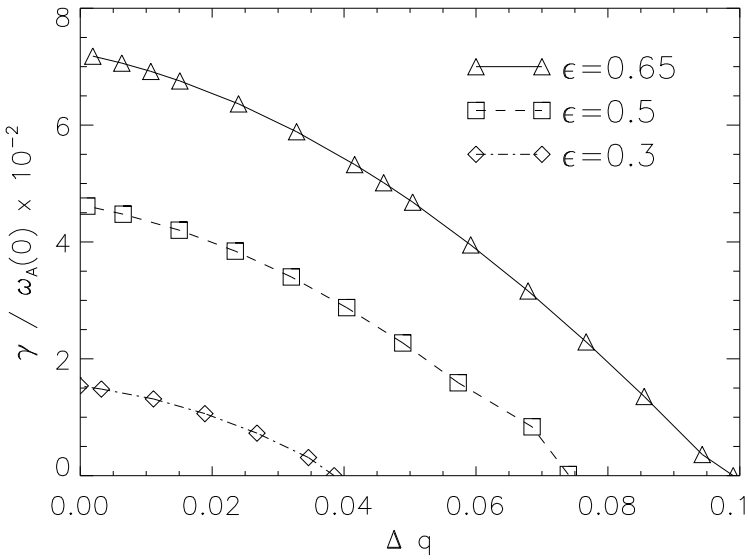

Figure 18. The growth rate of the $n = 1$ internal mode as a function of Δq for different inverse aspect ratios. Again, it is evident that tight aspect ratio devices are more susceptible to this saturated internal mode over a wider range of Δq.

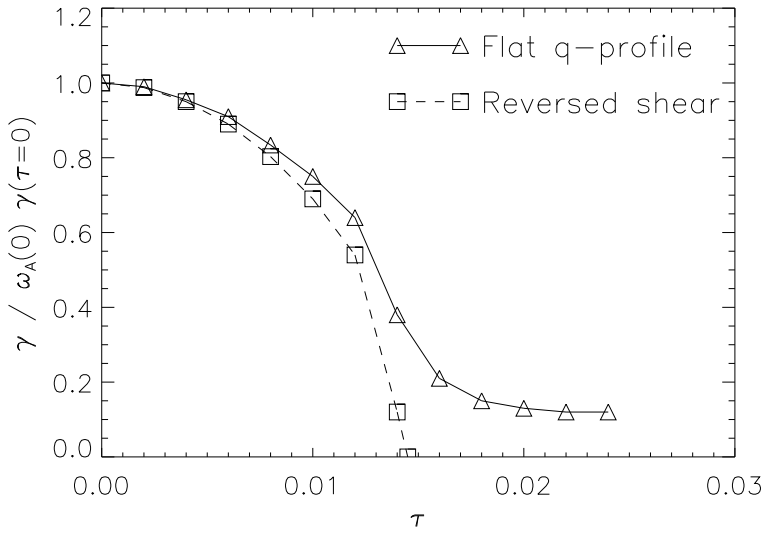

Figure 19. The growth rate of the $n = 1$ internal mode as a function of the ion diamagnetic frequency. Whilst the diamagnetism is stabilising, it does not completely suppress the mode.

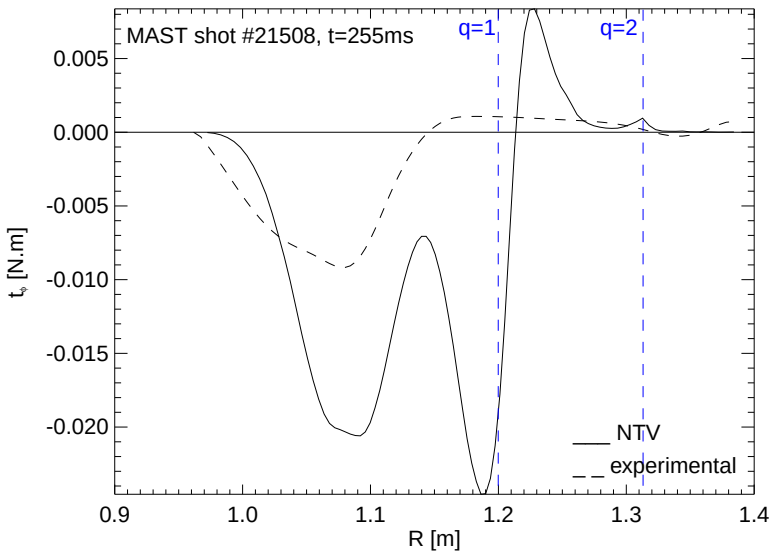

Figure 20. The torque predicted by NTV theory compared to the rate of change of angular momentum of the plasma as a function of major radius for MAST shot 21781.